Arch. Metall. Mater. **66** (2021), 1, 119-125

DOI: 10.24425/amm.2021.134767

YONG-JI ZHANG[1*], GUANG-LIANG WU[1], SHANG-WEN WU[1]

THE CRITICAL CONDITIONS AND KINETICS REQUIRED FOR DYNAMIC RECRYSTALLIZATION IN A HIGH-CARBON TOOL STEEL

A hot compression test was conducted on a Gleeble-3500 thermo-simulation machine to study the critical conditions and kinetics of dynamic recrystallization in a high-carbon tool steel. The critical conditions for the initiation of dynamic recrystallization were determined using the working-hardening theory. The quantitative relationship between the critical characteristics of dynamic recrystallization and the hot deformation parameters were elucidated based on two different methods:the apparent method and physically based method. It was found that the two methods both have high applicability for the investigated steel, but the physically-based method needs less parameters and makes it possible to study the effect of different factors. A dynamic recrystallization kinetics model was used to calculate the recrystallization volume fraction under different conditions. The calculation results matched well with the data obtained from the flow curves.

Keywords: high-carbon steel, critical conditions, dynamic recrystallization, work-hardening, kinetics model

1. Introduction

High-carbon steel 75Cr1 is currently one of the most widely used alloy tool steel. It is often used as a saw blade substrate in precise cutting machine, diamond circular saw blades, and special spring steels due to its excellent wear-resisting properties, good machinability and high thermal stability [1-2].

Dynamic recrystallization (*DRX*) can diminish the dislocation density, reduce the deformation resistance, refine the grain, control microstructural evolution and improve the hot workability of this steel [3-4]. Therefore, the determination of critical conditions is of great significance in the selection of the technological parameters necessary for industrial hot-working processes [5].

Dynamic recrystallization starts before the peak strain, but the critical strain (or critical stress) does not show significant characteristic such as a "single peak stress" on the flow curve, so it cannot be directly determined from the flow curve [6-7]. Although microstructural changes in metal materials can be used to determine the critical conditions for the initiation of DRX, this method requires that a large number of samples be subjected to critical conditions of *DRX* [8-10]. Therefore, some researchers have tried using different methods to predict the occurrence of *DRX*. For example, Ryan and McQueen [11] found that there was a stress peak in a constant strain rate flow curve such that an inflection point appeared at the curve of the strain hardening rate (θ) vs. stress (σ). Later on, Poliak and Jonas [8-9] showed that the inflection point corresponded to the appearance of an additional thermodynamic degree of freedom in the system which has been identified as dynamic recrystallization. Moreover, Najafizadeh and Jonas [12] simplified the previous method and the work-hardening rate vs. true stress curve was fitted using a third order polynomial equation.

To date, some researches have investigated hot-deformation behaviors and the constitutive relationship of 75Cr1 high carbon tool steel, but research studies on the critical conditions and kinetics of *DRX* are few. Therefore, the aim of this work is to determine the critical conditions for the onset of *DRX* in high-carbon tool steel. Furthermore, the relationship between critical conditions and hot deformation parameters obtained by introducing the Zener-Hollomon parameter. The strain of maximum dynamic softening will be obtained from the hardening rate-strain curve, which is used to calculate the volume fraction of *DRX*.

2. Experimental

The high-carbon steel with chemical composition of 0.75 wt.% C-0.33 wt.% Si- 0.7 wt.% Mn-0.42 wt.% Cr-0.25 wt.% Ni

[1] SCHOOL OF MINERALS PROCESSING AND BIOENGINEERING, CENTRAL SOUTH UNIVERSITY, CHINA

* Corresponding author: zhangyongji_csu@163.com

© 2020. The Author(s). This is an open-access article distributed under the terms of the Creative Commons Attribution-NonCommercial License (CC BY-NC 4.0, https://creativecommons.org/licenses/by-nc/4.0/deed.en which permits the use, redistribution of the material in any medium or format, transforming and building upon the material, provided that the article is properly cited, the use is noncommercial, and no modifications or adaptations are made.

was used in this work. Cylindrical specimens were machined into 8 mm in diameter and 12 mm in length. The hot compression tests were carried out using the Gleeble-3500 thermo-simulation machine in the temperature range of 900-1100°C at 50°C intervals, and strain rates ranging from 0.1 s^{-1} to 5 s^{-1}, up to the true strain of 0.7. The specimen was austenitized at 1200°C for 300 s. The specimen was then cooled down to deformation temperature at a rate of 5°C/s and held there for 120 s to ensure that the temperature became homogeneous. After the hot compression tests, the specimens were immediately water cooled to room temperature.

3. Results and discussion

3.1. Flow curves

Fig. 1 shows the true stress-strain curves of the studied steel under different experimental conditions. It can be seen from the figures that the deformation temperature and strain rate have a significant effect on the flow stress. As shown in Fig. 1(a)-(d), the peak stress and strain decrease with an increase in the deformation temperature or an decrease in the strain rate. This is because *DRX* is a heat-activated microstructure phenomenon that includes nucleation and growth. Increasing the deformation temperature increases grain-boundary mobility and accelerates the growth of dislocation-free grains [13-14]. In addition, an increase in strain rate reduces the time required to complete the deformation process while limiting the extent of grain growth after nucleation [15-16].

Moreover, most flow curves rise to peak stress and then gradually decline to steady-state stress. During the initial state of deformation, work hardening and dynamic recovery occur. However, the kinetics of work hardening is higher than that of dynamic recovery, which leads to a sharp increase in flow stress. When deformation proceeds to the extent that the internal metal dislocation density reaches a critical value, then the driving force for *DRX* is attained. The softening effect of *DRV* and *DRX* offsets a portion of work hardening. At the same time, the flow stress increases continuously, but the growth rate slows down

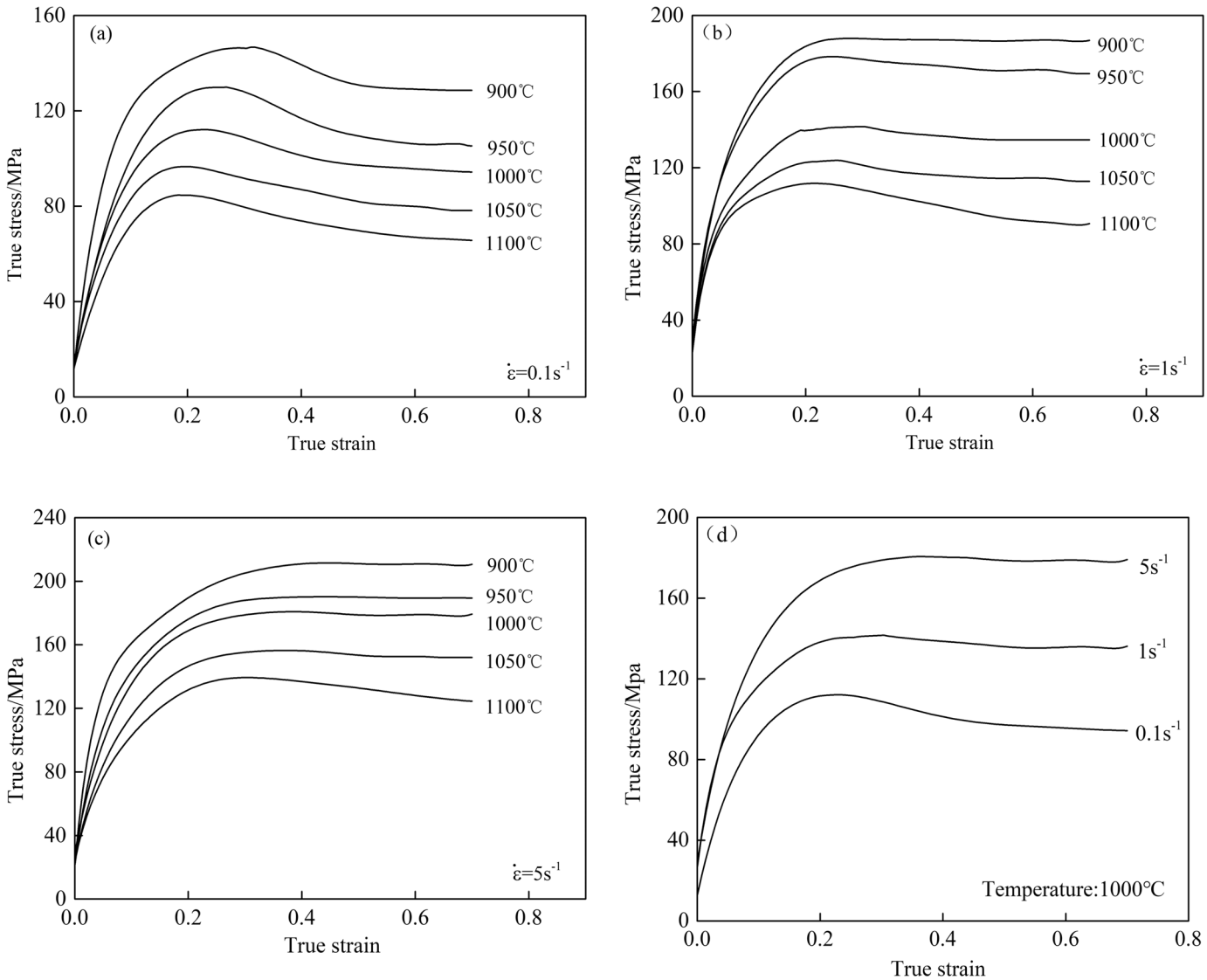

Fig. 1. Flow stress curves of 75Cr1 tool steel under different deformation conditions (a) 0.1s^{-1}; (b) 1 s^{-1}; (c) 5 s^{-1}; (d) 1000℃

and the flow stress reaches its peak value when the softening is in balance with work hardening. After reaching the peak stress, the flow stress gradually decreases to steady state stress (σ_{ss}), and the difference between peak stress (σ_p) and σ_{ss} reflects the kinetics of *DRX*. The greater the difference between σ_p and σ_{ss} is, the higher the kinetics of *DRX* is, so that the *DRX* offsets the effect of work hardening and softens the material to a lower stress level [12].

3.2. Critical stress and strain

As mentioned before,the critical conditions for the initiation of DRX cannot be determined directly from the flow curves. Najafizadeh and Jonas [8] found that the θ-σ relation curve can be adequately expressed as a cubic polynomial as follows:

$$\theta = A\sigma^3 + B\sigma^2 + C\sigma + D \tag{1}$$

where $\theta = d\sigma/d\varepsilon$ and A, B, C and D are constants for a given deformation temperature and strain rate.

The first derivative of Eq. (1) is

$$\frac{d\theta}{d\sigma} = 3A\sigma^2 + 2B\sigma + C \tag{2}$$

At the critical stress point, the second derivative value of Eq. (1) is zero, i.e.,

$$\frac{d^2\theta}{d\sigma^2} = 0 \Rightarrow 6A\sigma_c + 2B = 0 \Rightarrow \sigma_c = \frac{-B}{3A} \tag{3}$$

Fig. 2(a) shows the original θ-σ curve and the fitted θ-σ curve at the strain rate of 0.1 s^{-1} and different temperatures. It can be seen from the figure that the fitted curves are in good agreement with the original θ-σ curve. According to Eq. (3), the critical stress value (σ_c) under the corresponding deformation condition for the investigated steel can be calculated. The results are shown in Fig. 2(b) and the ratio of σ_C/σ_P is 0.89.

As noted earlier, at the inflection point of the lnθ-ε,

$$\frac{\partial^2\theta_c}{\partial\sigma^2} = 0 \tag{4}$$

where θ_c is the work hardening rate in the critical state for the occurrence of *DRX*, and

$$\frac{\partial\theta_c}{\partial\sigma} = \frac{\partial\theta}{\frac{\partial\sigma}{\partial\varepsilon}\cdot\partial\varepsilon} = \frac{\partial\sigma}{\theta\cdot\partial\varepsilon} = \frac{\partial\ln\theta_c}{\partial\varepsilon} \tag{5}$$

Thus,

$$\frac{\partial^2\theta_c}{\partial\sigma^2} = \frac{\partial^2\ln\theta_c}{\partial\varepsilon^2} = 0 \tag{6}$$

Therefore, the inflection point of the lnθ-ε curve also indicates the onset of *DRX*. In this work, the third order polynomial fitting of the lnθ-ε curve up to the peak strain at 900℃ and different strain rate is performed (Fig. 3(a)). Then the critical stress is calculated by using the above method to determine the critical stress. The results are shown in Fig. 3(b), and the ratio of $\varepsilon_C/\varepsilon_P$ is 0.43.

It can be seen from Fig. 2(b) and Fig. 3(b) that there is a good linear relationship between the critical stress (strain) and the peak stress (strain). In addition, the value of normalized critical stress (σ_c/σ_p) is in good agreement with the results that have been reported to be 0.875 [8], 0.84 [9], 0.89 [3], and 0.83 [16]. The value of the normalized critical strain ($\varepsilon_c/\varepsilon_p$), determined using the lnθ-ε curve, is 0.43. It should also be noted that for some steels, such as medium carbon alloy steel [16], and 17-4 PH stainless steel [3], the values of 0.47, 0.42 have also been reported in literatures. Therefore, the ratio of $\varepsilon_c/\varepsilon_p$ and σ_c/σ_p are in reasonable agreement with previously reported results.

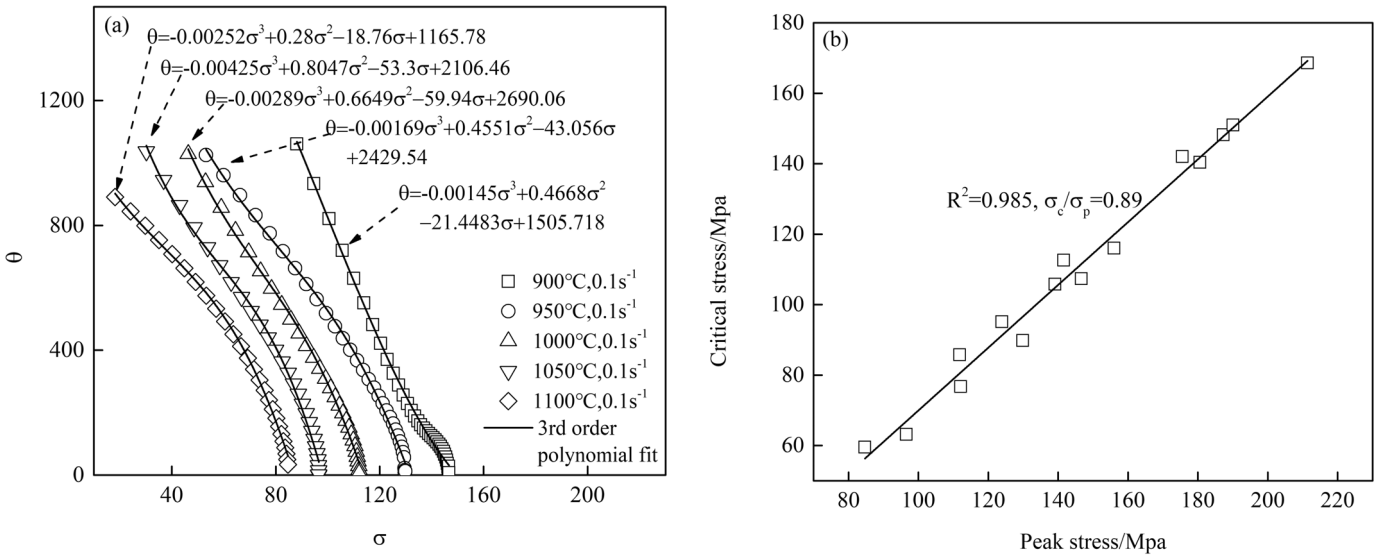

Fig. 2. The θ-σ curves at 0.1s^{-1} and different temperatures (a), relationship between critical stress and peak stress (b)

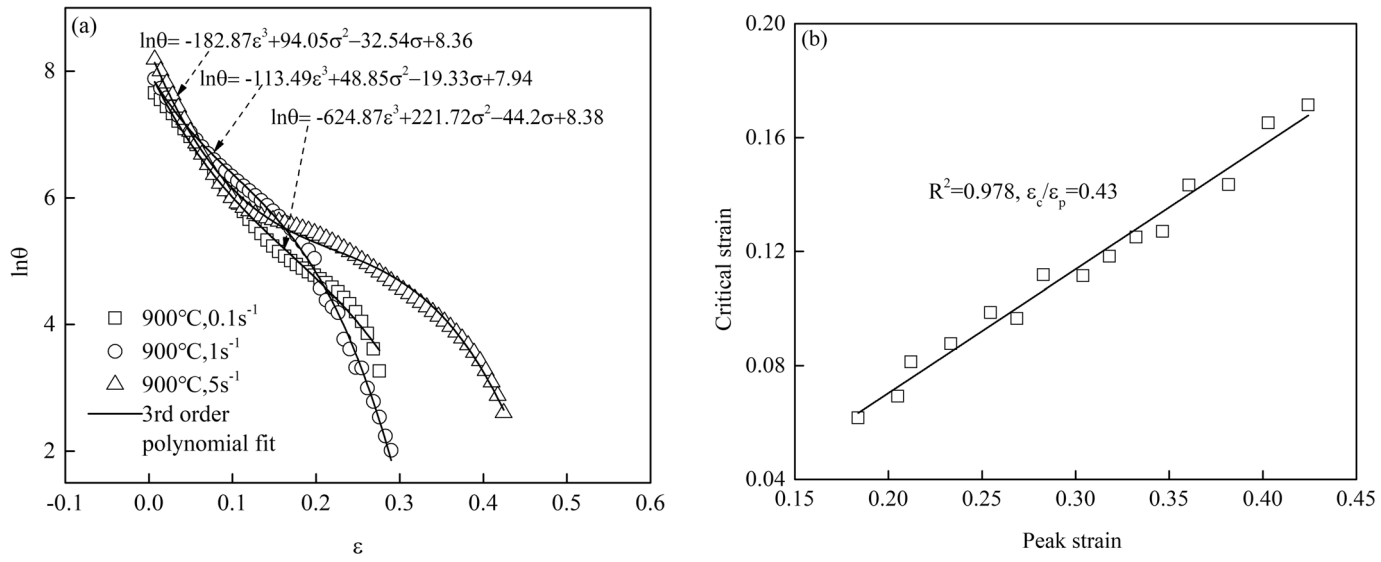

Fig. 3. The lnθ-ε curves at 900℃ and different strain rate (a), relationship between critical strain and peak strain (b)

3.3. The relationship between critical conditions and hot-deformation parameters

To further understand the dependence of these critical characteristics on the deformation parameters, it is necessary to introduce the Zener-Hollomon parameter:

$$Z = \dot{\varepsilon}\exp\left(\frac{Q_{act}}{RT}\right) = A[\sinh(\alpha\sigma)]^n \tag{7}$$

$$\begin{cases} Z = \dot{\varepsilon}\exp\left(\dfrac{Q_{act}}{RT}\right) = A_1\sigma^{n_1} & \alpha\sigma < 0.8 \\ Z = \dot{\varepsilon}\exp\left(\dfrac{Q_{act}}{RT}\right) = A_2\exp(\beta\sigma) & \alpha\sigma > 1.2 \end{cases} \tag{8}$$

Where $\dot{\varepsilon}$ is the strain rate (s^{-1}), σ is the flow stress (MPa), Q_{act} is the activation energy for deformation (J/mol). A, A_1 A_2, β, n, n_1 and $\alpha(\approx\beta/n_1)$ are material constants, R is the universal gas constant (8.314 J/mol/K).

Characteristic stresses such as peak stress, steady state stress,or stress corresponding to a specific strain can be used in these equations [4,17]. Since the peak stress can be attained from the flow curves precisely and easily, so in this paper peak stress was chosen to find the hot working constants. Taking natural logarithm of both sides of Eq. (7)-(8) respectively yields the following expressions for peak stress:

$$\ln\dot{\varepsilon} = \ln A + n\ln\left[\sinh(\alpha\sigma_p)\right] - \frac{Q_{act}}{RT} \tag{9}$$

$$\ln\dot{\varepsilon} = \ln A_1 + n_1\ln\sigma_p - \frac{Q_{act}}{RT} \tag{10}$$

$$\ln\dot{\varepsilon} = \ln A_2 + \beta\ln\sigma_p - \frac{Q_{act}}{RT} \tag{11}$$

Partially differentiating Eq. (9-11) at constant temperature respectively yields: $n = \left[\partial\ln\dot{\varepsilon}/\partial\ln\left(\sinh(\alpha\sigma_P)\right)\right]_T$, $n_1 = \left[\partial\ln(\dot{\varepsilon})/\partial\ln(\sigma_P)\right]_T$, $\beta = \left[\partial\ln(\dot{\varepsilon})/\partial\sigma_P\right]_T$. The value of n_1 and β can be derived from the average slopes of the plot of $\ln\dot{\varepsilon}$ versus $\ln\sigma_p$ and the slope of the plot of $\ln\dot{\varepsilon}$ versus σ_p, respectively. The value of n_1 and β are obtained as 8.48 and 0.062 respectively, as shown in Fig. 4 (a)-(b). Thus, the value of constant $\alpha(\alpha = \beta/n_1)$ can be obtained as 0.0073. As shown in Fig. 4(c), the value of n can be determined from the slopes of the plot of $\ln\dot{\varepsilon}$ versus $\ln[\sinh(\alpha\sigma_p)]$. The average value of n is calculated to be 6.33.

Partially differentiating Eq. (9) at a constant strain rate yields the following equation:

$$\left.\frac{\partial\ln\sinh(\alpha\sigma_p)}{\partial(1/T)}\right|_{\dot{\varepsilon}} = Q_{act}/Rn \tag{12}$$

The value of Q_{act} can be obtained from the slope of the plot of $\ln[\sinh(\alpha\sigma_p)]$ versus $1/T$, as shown in Fig. 4(d). The average value of Q_{act} is calculated to be 275.52 kJ/mol. Then, the relationship between Z and peak stress can be determined according to Eq. (7) as shown in Fig. 5(a) and can be expressed as follow:

$$Z = 4.21\times10^{10}\times\left[\sinh(0.0105\sigma_P)\right]^{6.33} \tag{13}$$

Recent research [17] showed that a constant hyperbolic sine power of $n = 5$ and self-diffusion activation energy (Q_{sd}) can be used to describe the appropriate stress. It can be seen that the deformation activation energy $Q_{act} = 275.52$ kJ/mol and it is close to the lattice self-diffusion activation energy ($Q_{SD} = 270$ kJ/mol). However, the hyperbolic sine power of n is 6.33 and it is quite different from the theoretical value of $n = 5$.

By consideration of the self-diffusion activation energy, the value of n is 5 only when the deformation mechanism is

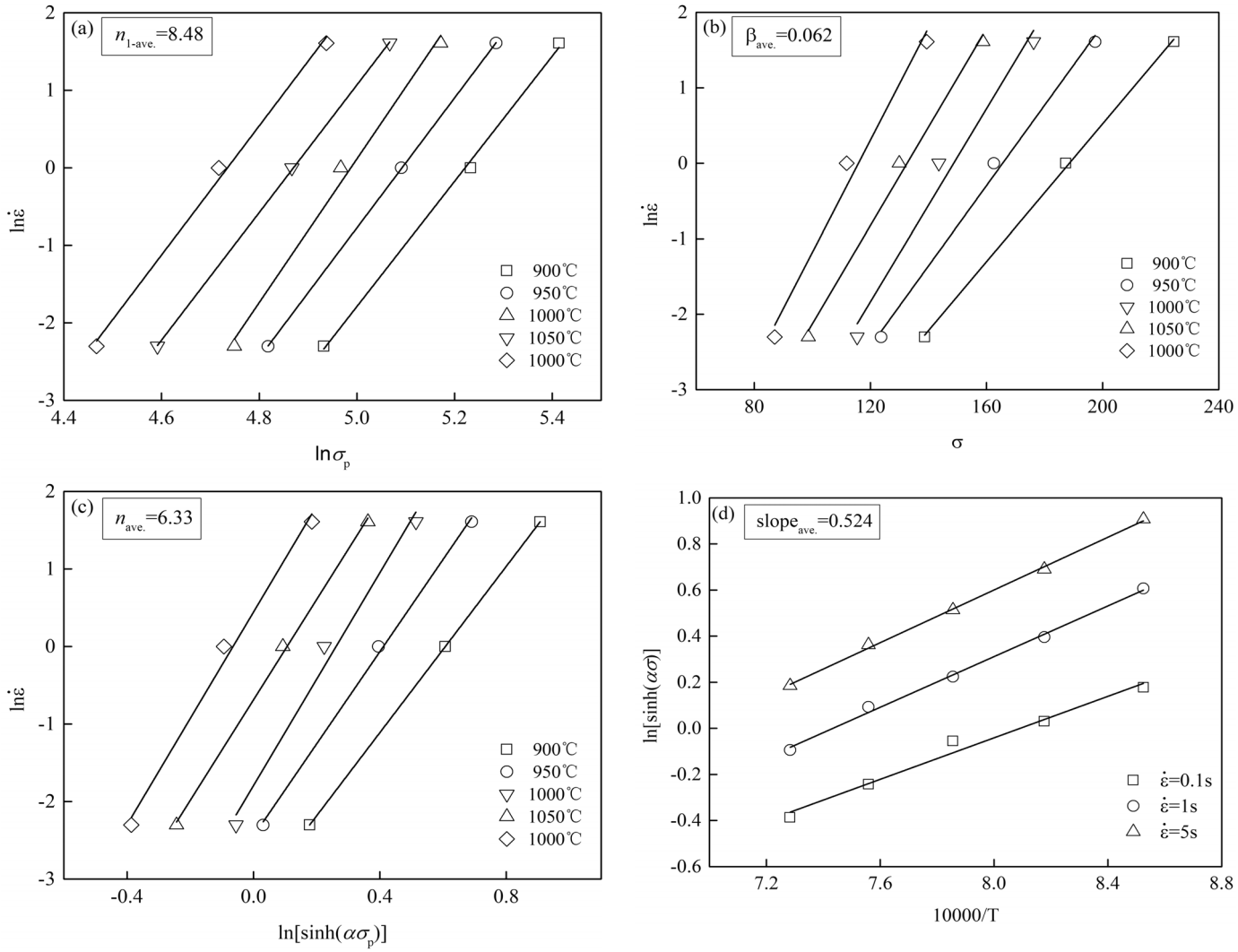

Fig. 4. Plot for calculation of (a) n_1; (b) β; (c) n; (d) Q_{act}

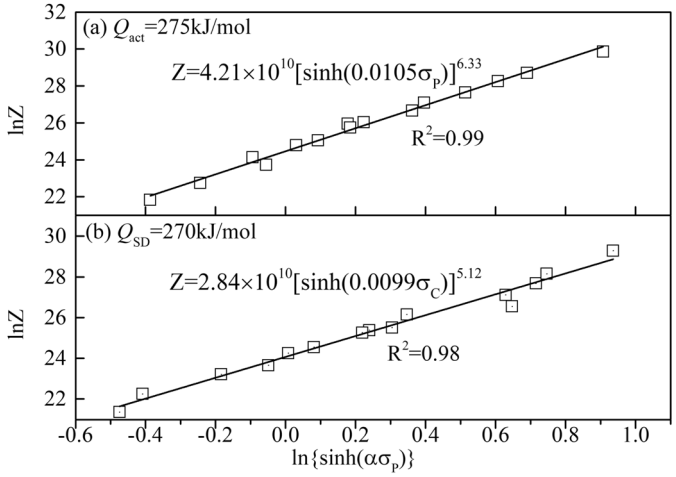

Fig. 5. Hyperbolic sine law analyses by consideration of σ_P and Q_{act} (a), σ_C and Q_{SD} (b)

controlled by the glide and climb of dislocations and thus the only softening mechanism considered is *DRV* [18]. Mirzadeh et al. [17] showed that the *DRX* process leads to a deviation of the value of n from the theoretical value. Since the critical conditions of *DRX* have been met before the peak stress, the *DRX* process has a certain influence on the peak stress. However, the material constant can be derived using the critical stress of initiation of *DRX* to bypass the effect of *DRX*, because the volume fraction of *DRX* is zero at the critical stress [18]. The critical stress values determined using the working-hardening theory are used for constitutive analysis. The value of β, n_1, α and n is determined as 0.068, 6.88, 0.0099 and 5.12, respectively. The hyperbolic sine law is applied by consideration of Q_{SD} = 270 kJ/mol and the results are shown in Fig. 5 (b) and the linear regression of the data results in the following equations:

$$Z = 2.84\times10^{10}\times\left[\sinh(0.0099\sigma_C)\right]^{5.12} \tag{14}$$

The calculated value of n = 5.12 is close to 5, which confirms that the deformation mechanism close to the critical point for the onset of *DRX* is controlled by the glide and climb of dislocations. The results show that the self-diffusion activation energy and the theoretical values of n = 5 can be used to describe the critical stress of *DRX* for the investigated steel. Although the consideration of the physical-based value of n and Q_{SD} may lead to some lack of precision for constitutive analysis, this makes it

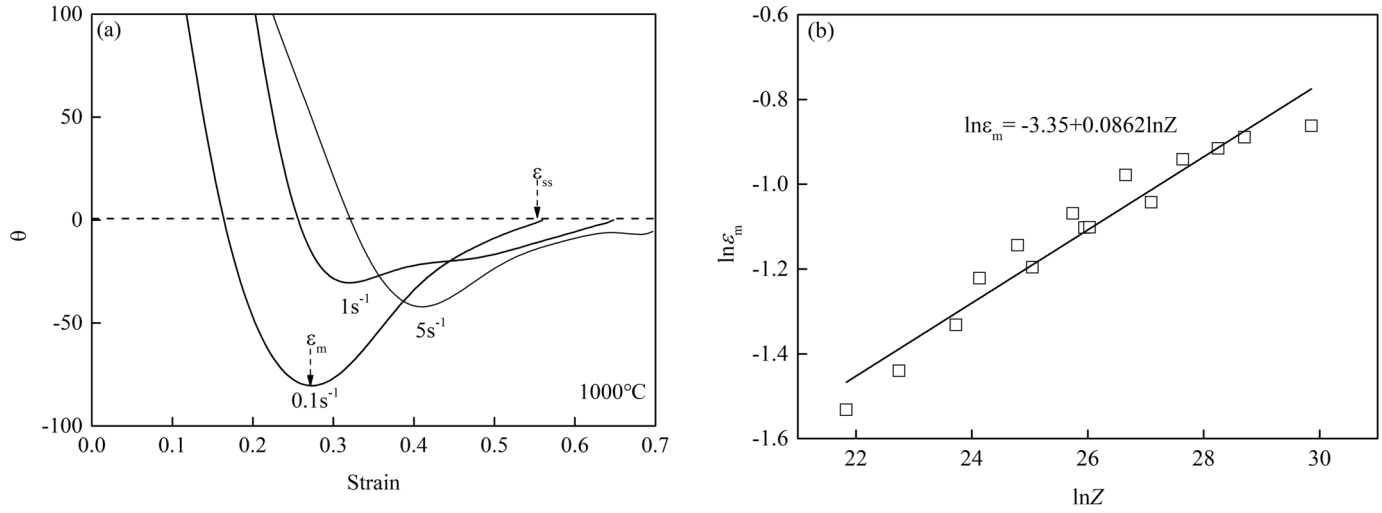

Fig. 6. Work-hardening rate vs. strain plots at 1000°C and different strain rate (a), dependence of the value of ε_m on the Z parameter (b)

possible to study the effects of different factors (such as carbon content [19], alloying element content and second phase particles [20]) on the flow stress and identify the rate control mechanism during thermal deformation [18].

3.4. The kinetics of dynamic recrystallization

The relationship between the volume fraction of dynamic recrystallization and plastic strain can be expressed in the follows [21]:

$$X_{DRX} = 1 - \exp\left[-0.693\left(\frac{\varepsilon - \varepsilon_c}{\varepsilon_m - \varepsilon_c}\right)^2\right] \quad (15)$$

where X_{DRX} is the volume fraction of *DRX*, ε is the true strain, ε_c is the critical strain, and ε_m is the strain corresponding to the maximum softening rate.

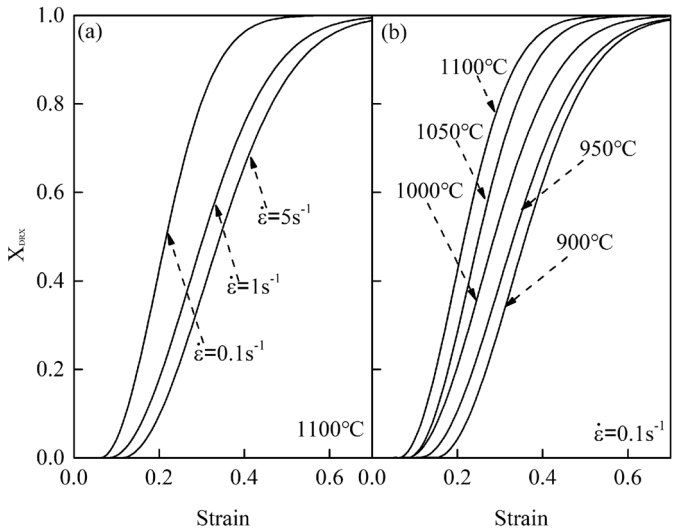

Fig. 7. Kinetics curves of DRX of high carbon tool steel: (a) 1100°C and different strain rates; (b) 0.1 s^{-1} and different temperatures

The relationship curves of work hardening with strain are shown in Fig. 6(a), and the minimum value of the curve corresponds to ε_m [22]. The value of ε_m under all experimental conditions can be obtained using this method and the dependence of ε_m on the *Z* parameter is shown in Fig. 6(b) and a regression analysis of this curve leads to the following equation:

$$\ln\varepsilon_m = -3.35 + 0.0862 \ln Z \quad (16)$$

Fig. 7(a)-(b) present the volume fraction of *DRX* as a function of strain at different strain rate with constant deformation temperature (1100°C) and different deformation temperature with constant strain rate (0.1 s^{-1}), respectively. Regardless of the effect of the deformation conditions, the volume fraction of *DRX* increases with strain due to the continuous nucleation and grain boundary migration [23]. Furthermore, as can be seen from Fig. 7(b), contrary to the effect of strain rate (Fig. 7(a)), the higher the deformation temperature, the smaller the plastic strain required to reach an equivalent recrystallization volume fraction, i.e., the greater the crystallization rate.

The work hardening rate and the volume fraction of *DRX* as a function of strain under the same conditions (1050°C and different strain rates) are compared to verify the accuracy of the kinetic recrystallization kinetic equation as shown in Fig. 8. In general, there will be two points for the zero of the work hardening rate on the θ-ε curves. When θ is zero for the first time, it indicates that the flow curve has reached the peak point. The second zero point of the work hardening rate will be appear due to the continuation of deformation which is the sign of the completion of recrystallization. Obviously, the second zero point of the work hardening rate, indicates the beginning of steady-state deformation, and the completion of the recrystallization ($X_{DRX} > 95\%$) [24]. Moreover, they appear almost at the same time. This confirms the model accurately predicted the dynamic recrystallization kinetics of the investigated steels.

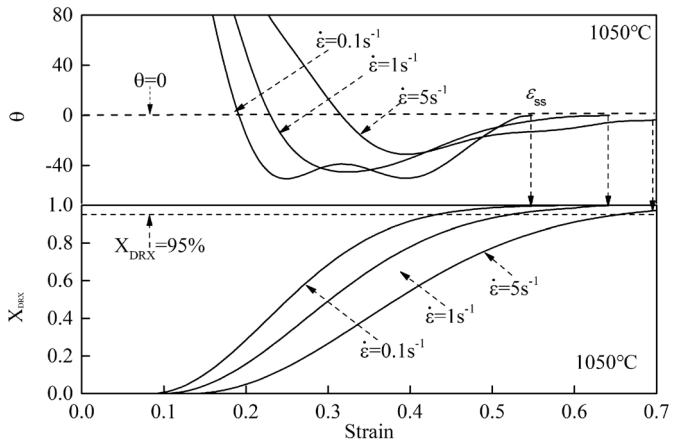

Fig. 8. Coincidence of the calculated value of X_{DRX} with the steady state strain

4. Conclusions

(1) Most of the high temperature flow curves of high carbon tool steel exhibited typical characteristics of *DRX* with a single peak stress followed by a gradual fall toward a steady-state stress.

(2) The ratio of σ_c/σ_p and $\varepsilon_c/\varepsilon_p$ are calculated using the hard-working method and are found to be 0.89 and 0.43, respectively. The calculated deformation activation energy of the high-carbon steel is approximately 275.52 kJ/mol.

(3) The relationships between the peak/critical stress of *DRX* and the deformation conditions are obtained by introducing the Z parameter based on two different methods.

(4) The value of ε_m is obtained by determining the minimum point on the θ-ε curve. This value is used to calculate the dynamic recrystallization volume fraction under different conditions utilizing an Avrami type dynamic recrystallization kinetics model. The calculated results are in good agreement with the steady-state strains that represent the completion of *DRX*.

REFERENCES

[1] S.T. Hu, H.Y. Chen, S.L. Li, G.B. Tang, Heat. Treat. Metals. **40** (8), 132-137 (2015).

[2] S.T. Hu, W.H. Yu, X.J. Lian, S.B. Zhai, Spec. Steel. **37** (1), 57-59 (2016).

[3] H. Mirzadeh, A. Najafizadeh, Mater Des. **31** (3), 1174-1179 (2010).

[4] S. Du, S. Chen, J. Song, Y.T. Li, Metall. Mater. Trans.A. **48** (3), 1310-1320 (2017).

[5] B.C. Zhao, G.Y. Li, F.L. Liu, X.M. Hu, L. Huang, Q.Y. Sha, Mater. Manuf. Process. **30** (10), 1235-1239 (2015).

[6] H. Mirzadeh, Metall. Mater. Trans. A. **46** (9), 1-11(2015).

[7] H. Jiang, J.X. Dong, M.C. Zhang, L. Zheng, Z.H. Yao, J. Alloys. Compd. **647**, 338-350 (2015).

[8] E.I. Poliak, J.J. Jonas, ISIJ. Int. **43** (5), 692-700 (2003).

[9] J.J. Jonas, E.I. Poliak, Mater. Sci. Forum. 426-432, 57-66 (2003).

[10] Solhjoo, Soheil, Mater. Des. **54** (2), 390-393 (2014).

[11] N.D. Ryan, H.J. Mcqueen, J. Mater. Process. Technol. **21** (2), 177-179 (1990).

[12] A. Najafizadeh, J.J. Jonas, ISIJ. Int. **46** (2), 1679-1684 (2006).

[13] M.R.G. Ferdowsi, D. Nakhaie, P.H. Benhangi, G.R. Ebrahimi, J. Mater. Eng. Perform. **23** (3), 1077-1087 (2014).

[14] H. Mirzadeh, J.M. Cabrera, A. Najafizadeh, Metall. Mater. Trans. A. **43** (1), 108-123 (2012).

[15] G.L. Wu, C.Y. Zhou, X.B. Liu, J. Cent. South. Univ. **23** (5), 1007-1014 (2016).

[16] B.C. Zhao, Z. Tan, G.Y. Lin, Q. Lu, Arch. of Metall. & Mater. **63** (1), 379-386 (2018).

[17] H. Mirzadeh, J.M. Cabrera, A. Najafizadeh, Acta. Metall. **59** (16), 6441-6448 (2011).

[18] H. Mirzadeh, M. Roostaei, M.H. Parsa, Mater. Des. **68**, 228-231 (2015).

[19] S. Saadatkia, H. Mirzadeh, J.M. Cabrera, Mat. Sci. Eng. A. **636**, 196-202 (2015).

[20] H. Mirzadeh, Mater. Des. **65**, 80-82(2015).

[21] G.R. Stewart, A.M. Elwazri, S. Yue, J.J. Jonas, Metal. Science. Journal. **22** (5), 519-524 (2006).

[22] A.M. Elwazri, P. Wanjara, S. Yue, Mater. Sci. Tech. **20** (11), 1469-1473 (2004).

[23] M. E. Wahabi, L. Gavard, F. Montheillet, Acta. Mater. **53** (17), 4605-4612 (2005).

[24] H. Mirzadeh, M. Roostaei, M.H. Parsa, Int. J. Mater. Res. **107** (3), 277-279 (2016).